



Open Archive Toulouse Archive Ouverte (OATAO)

OATAO is an open access repository that collects the work of Toulouse researchers and makes it freely available over the web where possible.

This is an author-deposited version published in: <http://oatao.univ-toulouse.fr/>
Eprints ID: 5529

To link to this article: DOI: 10.1039/c0jm04396f
URL: <http://dx.doi.org/10.1039/c0jm04396f>

To cite this version:

Roberts, Matthew and Johns, Phil and Owen, John and Brandell, Daniel and Edström, Kristina and El Enany, Gaber and Guéry, Claude and Golodnitsky, Diana and Lacey, Matt and Lecoeur, Cyrille and Mazor, Hadar and Peled, Emanuel and Perre, Emilie and Shaijumon, Manikoth M. and Simon, Patrice and Taberna, Pierre-Louis *3D lithium ion batteries— from fundamentals to fabrication*. (2011) *Journal of Materials Chemistry*, vol. 21 (n° 27). pp. 9876-9890. ISSN 0959-9428

Any correspondence concerning this service should be sent to the repository administrator: staff-oatao@listes.diff.inp-toulouse.fr

3D lithium ion batteries—from fundamentals to fabrication

Matthew Roberts,^a Phil Johns,^a John Owen,^{*a} Daniel Brandell,^d Kristina Edstrom,^d Gaber El Enany,^{†a} Claude Guery,^e Diana Golodnitsky,^b Matt Lacey,^a Cyrille Lecoer,^e Hadar Mazor,^b Emanuel Peled,^b Emilie Perre,^{cd} Manikoth M. Shaijumon,^c Patrice Simon^c and Pierre-Louis Taberna^c

DOI: 10.1039/c0jm04396f

3D microbatteries are proposed as a step change in the energy and power per footprint of surface mountable rechargeable batteries for microelectromechanical systems (MEMS) and other small electronic devices. Within a battery electrode, a 3D nanoarchitecture gives mesoporosity, increasing power by reducing the length of the diffusion path; in the separator region it can form the basis of a robust but porous solid, isolating the electrodes and immobilising an otherwise fluid electrolyte. 3D microarchitecture of the whole cell allows fabrication of interdigitated or interpenetrating networks that minimise the ionic path length between the electrodes in a thick cell. This article outlines the design principles for 3D microbatteries and estimates the geometrical and physical requirements of the materials. It then gives selected examples of recent progress in the techniques available for fabrication of 3D battery structures by successive deposition of electrodes, electrolytes and current collectors onto microstructured substrates by self-assembly methods.

1. Introduction

1.1 What is a 3D battery and why is it needed?

The microelectronics industry is continually downscaling its products to produce small devices such as medical implants, micro sensors, self powered integrated circuits or micro-electromechanical systems (MEMS).^{1,2} Such devices need rechargeable batteries with dimensions on the scale of 1–10 mm³ including all the components and all the associated packing. As

with all electronic technologies a high energy storage density is also required. This is one reason why a lithium ion system should be preferable as it will provide the highest energy density of available technologies suitable for the application. The recent surge in development of MEMS is therefore a particular driving force for development of a reliable and versatile lithium ion microbattery industry.

Thin film lithium ion microbatteries have emerged over the last 15 years or so^{3,4} as surface mountable devices up to about 10 μm thick. Current research in the provision of increased power levels to modern MEMS devices has become an increasing challenge because of the limited energy and power available per area of footprint on the substrate. Increasing the thickness does not solve this problem in a thin film cell because this also increases the current path length, leading to a reduction in power density. Conventional routes to solving this problem in the battery world would be to wind the thin film up, including a large surface area in a small volume. However, this is not suitable for most thin film systems as the components tend to be brittle and winding the

^aSchool of Chemistry, University of Southampton, Southampton, Hants, SO17 1BJ, United Kingdom. E-mail: jro@soton.ac.uk

^bSchool of Chemistry, Tel Aviv University, Tel Aviv, 69978, Israel

^cUniversite de Toulouse, CIRIMAT UMR CNRS, 5085, 118 rte de Narbonne, 31062 Toulouse Cedex 9, France

^dDepartment of Materials Chemistry, The Ångström Laboratory, Uppsala University, Box 538, SE-751 21 Uppsala, Sweden

^eLaboratoire de Réactivité et Chimie des Solides, UFR des Sciences, ALISTORE–European Research Institute, 80039 Amiens Cedex, France

† Now at Faculty of Engineering, University of Port-Said, Egypt.

Matthew Roberts from Buckinghamshire in the UK completed his MChem degree at the University of Southampton in 2004 with a placement at the National Physical Laboratory. He then began his PhD under the supervision of John Owen in the high-throughput study of lithium ion battery materials and completed in 2008 after an industrial placements at Matsushita Battery Industry, Japan. His postdoctoral work has been in the research of nanostructured materials and 3D battery architectures.

Phil Johns is originally from Cornwall in the UK and graduated from University of Southampton with a MChem degree in 2006. During his undergraduate studies he spent 6 months on industrial placement researching liquid crystal display technologies at Merck. Phil's final year project was within the Solid State Electrochemistry Group on platinum-infused Nafion membranes. He completed a PhD in nanostructured materials for energy storage in 2010.

electrodes will cause fractures breaks and short circuits. This limits these designs to planar systems which need large footprint areas for large capacities. This leads to the concept of *capacity per footprint area* ($\mu\text{A h cm}^{-2}$), which is a key consideration for the construction of microbatteries. Battery technologists typically characterise charge storage in terms of gravimetric (units mA h g^{-1}) and volumetric capacities (units mA h cm^{-3}). However, in the case of microbattery applications where the limitation is the area available, the relevant specification is capacity per footprint area.

The term “3D battery” can encompass many concepts. One definition⁵ reads “cells comprising anodes and cathodes which have active surface areas exposed in three dimensions”. Although this definition could include the composite electrodes used in the thick film (powder-binder composite) cells, it is normally reserved for cells assembled using micro-architected or micro-fabricated porous electrodes. We use the term “semi-3D” in this article to describe the combination of a micro-fabricated electrode (*i.e.* with three dimensionally exposed active area) connected to another electrode *via* a planar separator. A more advanced concept, herein called 3D, is a design which folds the complete thin film cell structure from the planar geometry into a thick laminate or network placed on a small footprint, so that and the overall current path remains small. Our analysis will include both of these concepts and show how they can improve device performance specifications. It will then discuss examples of cell designs and fabrication methods, with particular reference to materials deposition techniques.



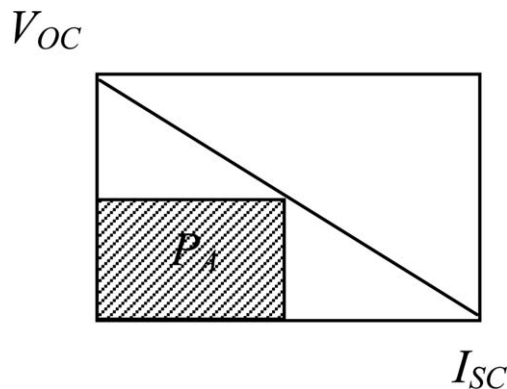
From left to right : John Owen, Matthew Roberts and Phil Johns

John Owen received his Ph.D. in Electrical Materials at Imperial College with Dr E.A.D. White and then worked in Solar Energy at the Materials and Energy Research Centre, Tehran, Iran. In 1979 he returned to Imperial College as a Wolfson Fellow with Prof. B.C.H. Steele on the Anglo-Danish Battery Project. His academic posts have been at the University of Salford then the University of Southampton where he continues to lead the Solid State Electrochemistry Group. Through his work on nanostructured battery materials he became a co-founder of Nanostructure PLC. His current research is now focused on, nanostructured current collectors and 3D cell architectures for high power charge and discharge of lithium batteries.

1.2 Power limitations in planar (2D) cells

1.2.1 Thin film cells. The term “thin film” usually refers to a planar semiconductor device that is made by physical or chemical vapour deposition, and the materials are solid ceramics or glasses. Thin film microbatteries (Fig. 1) are designed for small scale applications where high storage capacities are not required. Starting with a thin current collector, the cell is built by depositing layers of the lower electrode, electrolyte, upper electrode and a second current collector to form the battery. The thickness is limited to a few micrometres by the maximum thickness each layer can have before mechanical stresses cause fracture.

A major power limitation for the thin film cell is due to the Ohmic drop in the electrolyte/separator layer, which increases with the separator thickness, causing the maximum power to decrease. In the absence of other limitations we can estimate the maximum power available *per footprint (area)*, P_A from the resistance (R) \times area product as follows. The maximum power is delivered at half the short circuit current, I_{SC} where the Ohmic loss is half the open circuit voltage, V_{oc} .



$$R \times A = \frac{L_S}{\sigma_i} \quad (1)$$

and

$$P_A \sim \frac{V_{oc}}{2} \times \frac{V_{oc}}{2RA} = \frac{\sigma_i V_{oc}^2}{4L_S} \quad (2)$$

where σ_i = ionic conductivity, A = footprint area and L_S = separator thickness.

Alternatively, the Energy (E)/Power ratio can be expressed as a discharge time constant, τ ,

$$\tau = \frac{E_A}{P_A} \sim \frac{V_{oc} Q_A}{2} \times \frac{4L_S}{\sigma V_{oc}^2} \sim Q_V \times \frac{2L_S L_E}{\sigma V_{oc}} \quad (3)$$

where E_A and P_A are the specific energy and power per footprint, Q_A and Q_V are specific capacity (charge) of the electrode per footprint and volume, L_E is the electrode thickness.

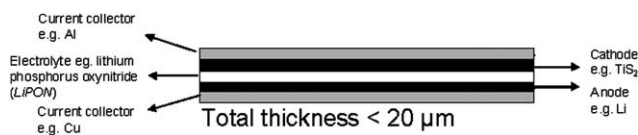


Fig. 1 Schematic diagram of a thin film cell.

Thin solid electrolytes like lithium phosphorus oxynitride (“LiPON”) and lithium borophosphate (“LiBP”)⁶ have been used, and despite their rather low conductivities (*e.g.* LiPON $\sim 10^{-5}$ – 10^{-6} S cm⁻¹) can support a modest current density due to their low thickness (<5 μm).

The energy available per footprint increases with the thickness of the cathode and anode layers. Increasing the electrode thickness will at some point lead to power limitations due to slow diffusion in the electrode rather than the low conductivity of the electrolyte. In that case we can estimate the maximum power using Fick’s laws according to the diffusion coefficient for lithium in the solid materials. The rate of diffusion determines the shortest discharge time for 50% discharge, $\tau_{0.5}$, and the corresponding maximum power density through the electrode thickness as follows:

$$\tau_{0.5} \sim \frac{L_E^2}{3D_{Li}} \quad (4)$$

where L_E is the electrode thickness and

$$P_A \sim \frac{0.5E_A}{\tau} \sim \frac{1.5E_A \times D_{Li}}{L_E^2} \quad (5)$$

The result is that for a given energy per footprint, the power per footprint and the maximum rate ($1/\tau$), for half discharge will both be inversely proportional to the square of the thickness. Low diffusion coefficients for lithium ions in solids will often limit the delivery of high energy and power simultaneously in a thin film construction

Bates *et al.*³ reported 50% DoD (degree of discharge) at rates of over 50 C (~ 70 s charge or discharge) using a cell of total thickness 15 μm with a LiCoO₂, LiPON electrolyte and Li counter electrode. Table 1 compares the result with the predictions of eqn (3) and (4) with typical parameter values reported in the literature. The table makes the point that micro dimensions can enable fast discharge even if the materials have very low conductivities and diffusion coefficients. However, although this level of performance is impressive, the total cell capacity is only 170 $\mu\text{A h}$ (taken at a rate of 1C). This means that although the cell can be charged and discharged very efficiently at high rates,

Table 1 Estimated discharge rate limitations due to electrolyte and electrode components of a thin film cell compared with the above data for a Li|LiPON|LiCoO₂

Performance of a LIPON thin film electrolyte, estimated compared with observed data	
σ_i/Scm^{-1}	1×10^{-6}
L_s/cm	3×10^{-4}
L_E/cm	2.5×10^{-4}
$Q_v/\text{C cm}^{-3}$	500
V_{oc}/V	4
Time constant τ/s	40
Experimental τ/s	70
Performance of a LiCoO ₂ thin film electrode, estimated compared with observed data	
$D/\text{cm}^{-12}\text{s}^{-1}$	10^{-10}
L_E/cm	2.5×10^{-4}
Time constant $\tau_{0.5}/\text{s}$	200
Experimental τ/s	70

only a small amount of charge and energy can be stored and therefore only small devices can be powered.

1.2.2 Thick film cells and composite electrodes. “Thick film technology” refers to the deposition of composite materials in layers from solvent dispersions, *e.g.* using doctor blade, laser coating or ink-jet equipment. The materials are usually ground to a small particle size and fabricated into composite porous electrode structures with a polymer binder to give the film mechanical strength. A liquid electrolyte contained in the pores provides ionic pathways and a conductive additive, typically acetylene black, provides electronic pathways to the surfaces of the active material particles where the redox reaction occurs. (The polymer can also be chosen to have a dual function as the binder and the electrolyte, *e.g.*, (polyethylene oxide (PEO)) containing a lithium salt (LiPF₆).⁷) Much thicker layers can be used in this case because the effective conductivity and diffusion coefficient for lithium are enhanced by the ionic conductivity of the infused electrolyte. Conventional lithium ion batteries found in applications such as mobile phones or laptops are typically formed from five flexible films 20–100 μm in thickness as shown schematically in Fig. 2.

An example of a thick film cell in the area of microbatteries was provided by Kim *et al.*⁸ who used a laser printer to deposit thick films of porous battery materials on to metallic current collectors, which were separated by a gel polymer electrolyte. Cathode and anode inks (LiCoO₂ and mesoporous carbon microbead (MCMB) respectively) were deposited onto their respective current collectors using the described laser printing process. The gel polymer electrolyte used was (PVdF-HFP/1M LiPF₆ in propylene carbonate (PC)/ethylene carbonate (EC)/dimethyl carbonate (DMC) (1 : 1 : 3)), supported with a laser-cut microporous polyolefin membrane separator. The rate performance of the cell was shown to be less dependent of the electrode thickness, in contrast to thin film sputtered cells where the rates of discharge decreased rapidly with electrode thickness. The authors briefly compared the capacity ($\mu\text{A h cm}^{-2}$) of the laser printed thick film microbattery to that of the thin film sputtered microbattery and reported low rate capacities that were an order of magnitude greater for the laser printed system.

In the above case the improvement was probably due to the higher conductivity of the gel polymer electrolyte compared with that a glass or ceramic. A similar situation exists when a liquid electrolyte contained in porous polymer—the current path is essentially perpendicular to the plane of the separator on the microscopic scale. Provided that the microscopic path is relatively non- tortuous, we can use eqn (2) as a reasonable prediction of the power limitation due to the electrolyte resistance.

Accurate estimation of the power limitation due to diffusion in composite electrode materials is a complex calculation that is outside the scope of this discussion, but useful estimations can be made in some limiting cases. For example, if *solid state* diffusion is the limiting factor we now have a discharge time that depends on the particle *radius* R rather than the electrode thickness:

$$\tau_D \approx \frac{R^2}{D_{Li}} \quad (6)$$

Reduction of the particle size of the electrode material can, in principle, alleviate the problem of solid state diffusion, so that

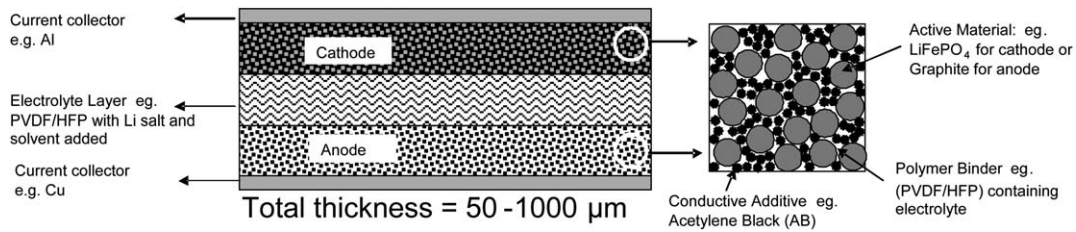


Fig. 2 Schematic diagram of a thick film cell.

the power density should only be limited by ion and electron transport in the *composite*. Generally we can estimate a composite diffusion coefficient D_{comp} using the De Levie expression,⁹

$$D_{comp} = \frac{(\sigma_i \cdot \sigma_e)}{C_v(\sigma_i + \sigma_e)} \approx \frac{\sigma_i}{C_v} \text{ for } \sigma_e \gg \sigma_i \quad (7)$$

where σ_e , σ_i are electronic and ionic conductivities and C_v is the pseudocapacitance per unit volume.

In the latter case the power per footprint area decreases with the electrode thickness as in eqn (4) and we again obtain a limitation in the electrode thickness which limits the storage capacity as before because of the need to retain a specified power per footprint area.

Generally, the low diffusivity of solid electrodes is bypassed by the liquid or polymer electrolyte of the composite provided that the electrode particles are small enough and the electrolyte is sufficiently conductive.

Another limiting factor that can become dominant during fast discharge of composite electrodes is the limited rate of *salt diffusion* in the composite.¹⁰ The following approximation was suggested to estimate this effect.

$$\tau \sim \frac{L^2}{D_{salt}} \times \frac{(1 - T_+)[Li]}{[salt]} \quad (8)$$

where $T_+ = Li^+$ transference number, or the number of moles of Li crossing per Faraday of charge passed, $[Li]$ = change in lithium concentration in the electrode during discharge, $[salt]$ = salt concentration in the separator. Obviously, if the transference number for cations is close to one, as it is believed to be for many solid and glassy electrolytes, this limitation will not apply.

Again we have a simple expression that approximately quantifies the common result that for a given time constant for discharge, the ionic conductivity required of the electrolyte within the composite varies as the square of the electrode thickness, L^2 . Therefore, we can enable the use of relatively low conductivity electrolytes *e.g.* dry polymers or glasses; by reducing the electrode thickness by just one order of magnitude we can compensate for a reduction in conductivity by two orders of magnitude. Such a reduction in thickness, however, will reduce the energy density per footprint as in the thin film cell. Therefore, for applications that require both high power and energy per footprint, or for devices constructed with a poorly conducting, liquid-free electrolyte we seek a method of constructing a thick cell with a short ionic current path between the two electrodes. Several examples of this will be found in the principles and descriptions of the 3D cells described below.

1.3 Semi-3D and 2D microbatteries and models

The following section examines some microbattery architectures that illustrate the development of thin film technology towards the full 3D configurations described in section 1.4.

1.3.1 Nano-architected current collectors and “semi-3D” cells.

Several types of nano-architected electrodes have been described as alternatives to the composite electrode described above. They may be defined here as electrodes that are carefully fabricated to optimise the ionic and electronic current paths, *e.g.* as shown in Fig. 3, by depositing a thin layer of active material on a nano-architected current collector array. The design will ensure a small tortuosity factor, leading to a higher effective diffusion coefficient than that obtainable from a random composite electrode. The theory of the composite electrode presented above may be applied most easily to the example of Fig. 3 because the *effective* ionic conductivity due to the electrolyte within the channels is precisely the bulk conductivity value multiplied by the ratio of the cross-sectional area of the ionic current path to the total area of the base current collector.

Fleischauer *et al.*¹¹ used a high-vacuum physical vapor deposition technique to deposit porous thin films of high aspect ratio silicon posts. Fig. 4 shows the film of silicon posts roughly 500nm in height deposited on a single crystal silicon wafer (the deposited silicon was shown to be amorphous by XRD).

Cells that could be classified as semi-3D were made by combining the porous Si with 1M LiPF₆ in EC:DMC (1 : 2 vol: vol) electrolyte and lithium foil as the counter electrode. The cells were cycled at C rates of roughly C/8, C/4 and C/2 for 10 cycles at each C rate before repeating the pattern. Good capacity retention was reported (after the initial insertion) at all three rates and most capacity loss associated with higher-rate cycling was recovered as the C rate was reduced, the rate capability was attributed to the porosity of the silicon films.

Teixidor *et al.*¹² presented the fabrication and characterization of carbon pillars as electrodes for lithium ion microbatteries. The authors used lithographic patterning and subsequent pyrolysis of

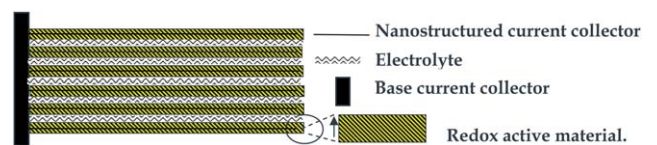


Fig. 3 Schematic diagram of a 3D nanostructured current collector coated in redox active material. This makes a “Semi-3D cell” when coupled with a second electrode *via* a planar separator.

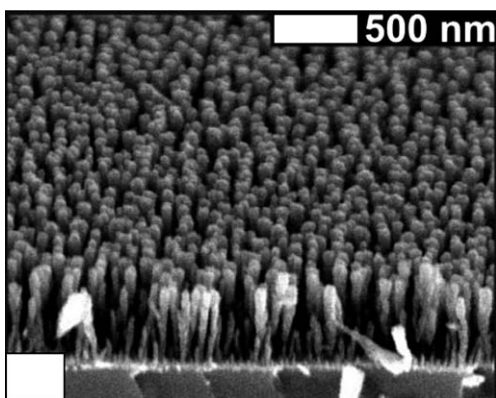


Fig. 4 SEM of 500 nm thick Si films deposited on a Si(100) wafer. Reprinted with permission from ref. 11.

the cross linked photoresist to produce a variety of different shaped carbon pillar current collectors onto which MCMB's were spin coated from a solvent dispersion. By using the photoresist as a solvent it was possible to enhance the adhesion of the MCMB particles onto the polymer microstructures by curing the dispersion with UV light.

An example of a semi-3D cell is given the microstructured cathode in a semi-3D cell is the approach by Tonti *et al.*¹³ and Park *et al.*¹⁴ involving the concept of using three dimensionally macroporous LiMn_2O_4 as cathodes. The preparations typically start with the fabrication of an opal template using polystyrene spheres. This template is then filled with a sol gel preparation mixture for LiMn_2O_4 . The composite is calcined in air and the polystyrene beads are removed *via* combustion. These inverse opal structures gave a large area gain per layer of spheres, with each added layer an increase in surface area of pi is given.

It must be emphasised that the pore size of the electrode structure in a semi-3D cell does not need to be large enough to accommodate another electrode by interdigitation—all that is required is electrolyte penetration. In that case, all the reports of nanostructured electrodes^{15,16} can be considered as the basis of semi-3D cells.

1.3.2 Two-dimensional batteries with interdigitated electrodes.

Given a fine enough nanostructure, the semi-3D configuration can deal effectively with the problems of low diffusivity in the solid state. However, it does not compensate for a poorly conducting electrolyte—that can only be done by reducing the ionic path through the electrolyte, *e.g.* by an interdigitated electrode geometry. This was achieved by Dokku *et al.*¹⁷ using an interdigitated microarray of gold current collectors, coated with $\text{LiMn}_2\text{O}_4/\text{Li}_{4/3}\text{Ti}_{5/3}\text{O}_4$ and a gel-polymer electrolyte. Photolithography was used to pattern a SiO_2 substrate with microarrays of gold current collectors. Sol-gel precursors of LiMn_2O_4 and $\text{Li}_{4/3}\text{Ti}_{5/3}\text{O}_4$ were then deposited onto the current collectors, using a micro injection system, before the precursors were calcined to form the electrode materials. Thermal polymerization of methyl methacrylate in the presence of 1M LiClO_4 EC:DMC (1 : 1) electrolyte gave a sheet of gel polymer electrolyte based on poly(methyl methacrylate) (PMMA) and LiClO_4 , this was placed onto the microarray of LiMn_2O_4 and $\text{Li}_{4/3}\text{Ti}_{5/3}\text{O}_4$ and a lithium

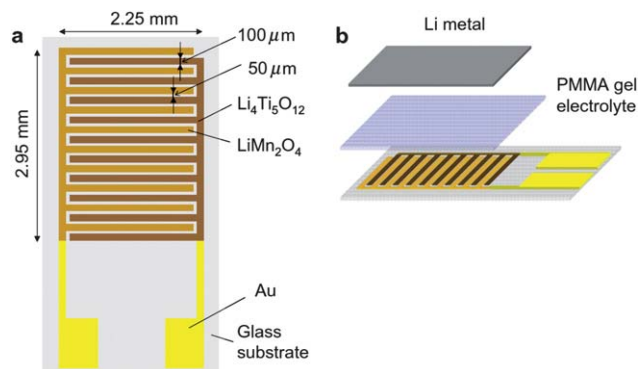


Fig. 5 Schematic illustrations of microarray electrodes of LiMn_2O_4 and $\text{Li}_{4/3}\text{Ti}_{5/3}\text{O}_4$ (a), and assembly of electrochemical cell (b). Reprinted with permission from ref. 17.

foil was placed on top for initial conditioning and individual electrode characterisation (Fig. 5).

The cell showed charge and discharge plateaus of 2.55 and 2.4V respectively. A performance of >50% DoD was seen at 50 C (~1 min charge discharges). The authors noted that although the system had a good rate performance, which they attributed to the ionic conductivity of the polymer electrolyte and the short diffusion path of the lithium ions, the energy density compared unfavourably to thin film sputtered systems. Shortening the distance between the microelectrode arrays and increasing the thickness of the electrodes were suggested as possible methods of improving the energy density.

An interdigitated electrode cell with efficient current collectors under the electrodes can be modelled approximately by considering a parallel combination of several thick film cells. However, a numerical simulation gives more accuracy, and in particular deals with the additional rate limitations due to the current collector resistance. The electrochemical processes in both the electrolyte and electrodes in the interdigitated configuration were modelled by Zadin *et al.*^{18,19} who used a Finite Element Analysis (FEA). Such a model can also be used to study the performance of 3D-microbatteries with a “trench” architecture, currently under study by Notten *et al.*²⁰⁻²² The FEA simulations of 3D-cells of graphite, 1 M LiPF_6 in EC/DEC and LiCoO_2 in the trench-model geometry were performed using concentrated solution theory, Maxwell-Stefan diffusion and Butler-Volmer kinetics. In addition to modelling the overall discharge characteristics, the model showed large non-uniformities are arising in the current distribution depending both on architecture—trench depth, trench separation, plate shape (Fig. 6)—and on material selection. Since a non-uniform activity on the electrode/electrolyte interface results in a non-uniform utilization of the active material, these factors have substantial effects on the charge/discharge profile of the batteries. Thus, a non-optimal battery design leads to a non-optimal current distribution and electrode activity, and thus to an underutilization of the active material. At the beginning of the discharge cycle, the delithiation and lithiation of the electrodes starts directly from the plate tips in the trench-cell, leading to a fast depletion and accumulation of Li ions in these regions of the electrodes. This is due to the inhomogeneous current density distribution, in turn caused by the

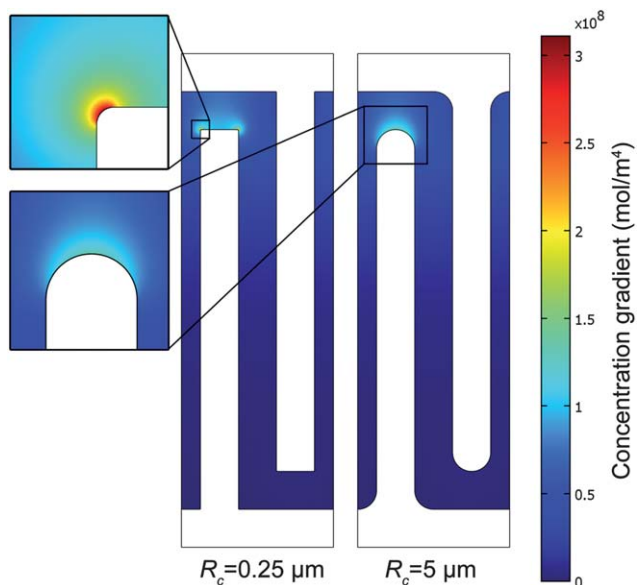


Fig. 6 Calculated concentration gradient at steady-state for different corner radii at the electrode plate ends; the inserts are magnifications. The high concentration gradient for sharp corners indicates non-uniform material utilization. Reprinted with permission from ref. 18.

electrode tip being considerably smaller than the corresponding surface of the opposite plate, making the current density concentrated to the tips – a direct effect of the interdigitated design. Consequently, the higher local reaction rates at the plate tips will limit the current through the battery. The current then has to find a different route through the cell, which ends the electrochemical processes prematurely, at less than 70% state-of-charge. In addition to the above effect, it may be anticipated that inhomogeneous expansion and contraction of the electrode material could result in cracking and disconnections of the electrode leading to poor capacity retention on cycling. Since the battery performance depends on global architecture, local geometrical design and material selection, there is clearly a need for systematic optimization using FEA modeling.

1.4 Three-dimensional microbattery designs and fabrication methods

Several designs have been proposed.^{2,1,19} They are all based on the five-layer concept of Fig. 1, in which the current collectors form two closely-spaced interpenetrating networks and the

electrode/electrolyte/electrode sandwich forms the interface separating the two current collectors shown in black and red. The power density may again be estimated from the eqn (1)–(5) above by recognising that neither the thickness of the electrode L_E nor the separator, L_S , can exceed the spacing between the positive and negative current collector. Two main topologies can be distinguished as interdigitated or interlocked as shown in Fig. 7 (a) and (b).

Further differences arise from the detailed geometric arrangements and fabrication methods for the interdigitated or interlaced topology. The easiest concept to visualise is that of Fig. 7(a) where the two dimensional diagram can represent either a cross section through an array of interpenetrating trench structures as in a thick version of the 2D cell described above or two arrays of interpenetrating columns as current collectors. In either case the first two layers, an active material (cathode or anode) and an electrolyte/separator are deposited conformally, leaving enough space for a current collector of the opposite polarity to the base. One problem here is to optimise the fabrication of the final two layers - in particular how to ensure that the space left after deposition of the second active material is sufficient and precise to ensure continuity of the final current collector if it is required to compensate for a poorly conductive active material. Fig. 7(b) shows the aperiodic sponge approach where the layers are deposited on a reticulated surface. In this case the two electrodes are non-separable because they are interlocked.

An alternative approach has been based on the high aspect ratio electrode array system proposed in previous papers by Min *et al.*²³ and others.^{24,25} Two independent and isolated current

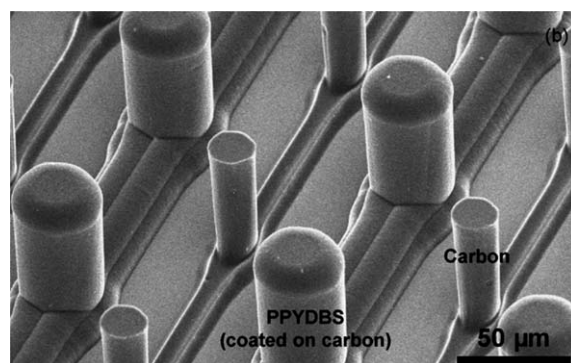
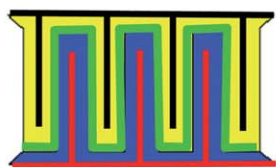
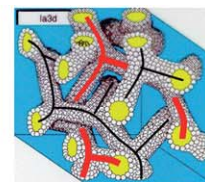


Fig. 8 Carbon and PPYDBS electrodes on individual current collector arrays. Reprinted with permission from ref. 23.



(a) interdigitated or interlaced topology



(b) interlocked or sponge topology where two electrode networks fill each others' pores.

Fig. 7 Two topologies for the 3D microbattery.

collector arrays of carbon for the cathode and anode were produced by photolithography. The carbon tracks and high aspect ratio pillars were produced from pyrolysis of cross linked polymer based photoresists. Dodecylbenzenesulfonate doped polypyrrole (PPYDBS) was electrodeposited onto one of current collector arrays to form a cathode; the second array of carbon pillars was used as the anode and 1M LiClO₄ in 1 : 1 EC-DMC electrolyte completed the battery. Fig. 8 shows the completed arrays of carbon and PPYDBS electrodes on their individual current collectors.

The authors compared the gravimetric capacity of half cells of the 2D and 3D PPYDBS electrodes and found the 3D configuration to have slightly better performance (37.9 mAh g⁻¹ at 1.15 C for the 3D and 23.4 mAh g⁻¹ at 0.9 C for the 2D configuration). The increase in performance of the 3D PPYDBS electrodes was attributed to the larger active surface area and the effect of the electrolyte penetration into the entire electrode as compared to the planar front that the electrolyte makes with the 2D PPYDBS electrode. Albeit a good demonstration of the 3D concept as intended, the capacity per footprint was only 11 μAh cm⁻² and further problems were found with electronic short circuits leading to self discharge, and large internal resistances attributed to the carbon current collector arrays.

Fig. 7(b) shows an isotropic 3D configuration that can be also be fabricated by successive deposition of conformal films. It illustrates the fact that a layer-by-layer approach can be applied to a surface of any shape or topology. This fact was realized by Nathan *et al.*²⁶ who used a different substrate geometry in one of the first reports of a ‘functioning full 3D’ lithium ion microbattery. The structure was based on a planar substrate with high aspect ratio channels, *e.g.*, glass or silicon ‘micro channel plates’ (MCP, essentially silicon or glass wafers perforated by a regular

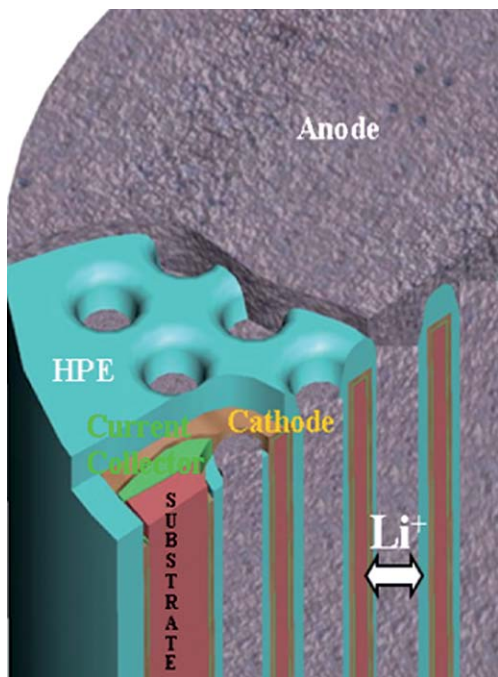


Fig. 9 Schematic view of a 3D microbattery showing the substrate (perforate silicon), current collector (Au or Ni), cathode (Cu_x, etc), hybrid polymer electrolyte and anode.

array of microchannels). Five layers were deposited successively to make the structure. The base current collector was formed by electroless deposition of a thin layer of Ni on the channel walls to be covered by electrodeposition of a conformal layer of molybdenum sulfide as the cathode. Next a polymer electrolyte separator based on PVDF was deposited onto the molybdenum sulfide through the depth of the microchannel using what was described as ‘sequential spin-coating and vacuum pulling steps’. An anode of mesoporous microbeads MCMB with polymer binder was deposited from a solvent slurry into the microchannel using sequential spin-coating and vacuum pulling steps. Electronic connection to the cathode was made by back polishing the anode and polymer electrolyte to reveal the Ni cathodic current collector. Lithium foil placed on top of the structure provided lithium intercalation into the anode. Once constructed the whole assembly shown in Fig. 9 was soaked in 1M LiPF₆ 1EC:1DEC or 1M LiBF₄ 1 EC: 9 DEC under vacuum for 10 h. The measured capacity of 1 mAh cm⁻² was much greater than the 2D equivalent, due to the area gain from the 3D structure.

Kotobuki *et al.*²⁷ constructed a microbattery based around a ‘honeycomb’ structured Li_{0.35}La_{0.55}TiO₃ (LLT) solid electrolyte. The schematic ‘honeycomb’ type configuration (Fig. 10) shows a bidirectional pore structure.

Sol-gel precursors of the cathode and anode materials LiCoO₂ and Li₄Mn₅O₁₂ were injected (vacuum impregnation) into opposing sides of the microstructured electrolyte, and subsequently calcined to form the full 3D microbattery (Fig. 11).

The full LiCoO₂/LLT/Li₄Mn₅O₁₂ was successfully assembled and tested; the cell exhibited a discharge voltage of ~1V but as with the cathode and anode half cells, showed a very low discharge capacity of 7.3 μA h cm⁻², stated as only 0.1% utilization of the limiting LiCoO₂ electrode. The authors attributed

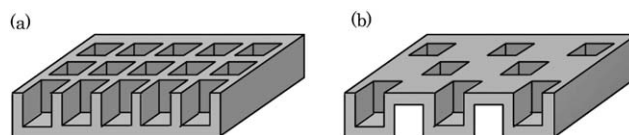


Fig. 10 Illustration of LLT honeycomb structures, (a) Half honeycomb structure with 400 holes on one side of LLT membrane and (b) full honeycomb structure with 200 holes on each side of LLT membrane. The hole size is 180 μm × 180 μm × 180 μm. Reprinted with permission from ref. 27.

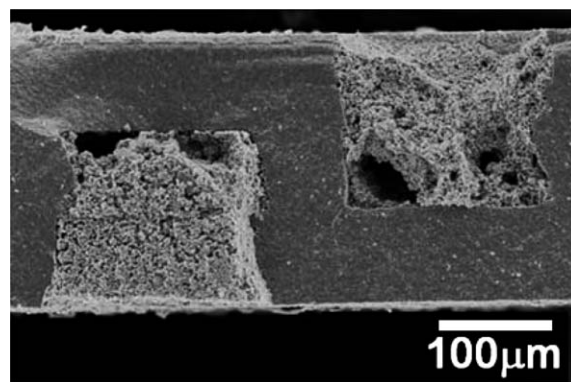


Fig. 11 Cross section of LiCoO₂/LLT/Li₄Mn₅O₁₂ cell. Reprinted with permission from ref. 27.

the poor performance microbattery to several factors; firstly high contact resistance between the walls of the microstructured electrolyte and the active material, and secondly size of the ‘honeycomb’ electrolyte. The depth of the pores in the electrolyte was 180 μm , meaning a large diffusion distance of the lithium ion from the centre of the pore to the electrolyte. The authors noted that a reduction in the size of the electrolyte pore should improve the available capacity of the system.

1.5 Summary of 3D battery principles

It may be seen from the above examples that 3D battery fabrication first requires microfabrication of the base array to act as the mechanical support and, in some cases, to double as a current collector or separator. After that, the challenge is to develop an armoury of deposition techniques for the other layers of current collectors, active materials and electrolytes. In particular we can see the need to distinguish *conformal* and *pore-filling* deposition techniques. For fabrication by sequential coating we need conformal deposition of the first electrode to provide a uniform electrode of the desired thickness. Similarly, for electrolyte deposition we need a very thin conformal deposit but it is essential to avoid pinholes that could act as short circuit paths for electrons to pass directly between the electrodes. The last deposited layer should be pore filling to make use of the available space in a continuous current path.

The thickness of each layer of the 3D construction is an important design consideration. Although minimising the thickness of the layers maximises the power, avoidance of pinholes in the separator will probably require a layer at least a micrometre thick. This estimate of the length scale, coupled with the need to maximise the volume fraction of the active materials, leads to a scale of up to tens of microns for the active material layers. The final current collector layer (or the second electrode material itself if sufficiently conducting not to require a current collector) presents a conflict between a thin structure to provide enough space for active material and a thicker design for a continuous current path.

3D nanostructured electrodes are required to compensate for low diffusion coefficients in solids, and to alleviate problems due to decrepitation of brittle solids during cycling. Here, the inter-columnar scaling can be much smaller than that of the 3D cell array. Generally, smaller is better, and the only other considerations are dimensional effects on the conduction paths, *e.g.* restricted electrolyte penetration into small pores, and problems of interfacial instability or irreversible capacity that increase with the interfacial area.

2. Microfabrication and deposition of battery components

2.1 High aspect ratio substrates and current collectors

The first requirement of any 3D microbattery system is to have a substrate and current collector which the three layers of battery material can be deposited onto.

Cu has long been used as a current collector for the anode where it is cathodically protected from corrosion.²⁸ Arrays of free standing copper nanorods have been produced directly on copper disk substrates, by electrodeposition inside the pores of

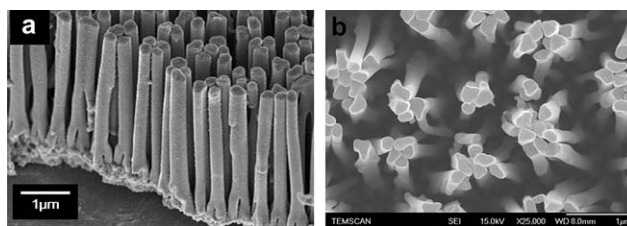


Fig. 12 SEM images of a) a cross sectional view of Cu-nanorod current collectors grown directly on to Cu substrate and b) a Ni nanorod array directly grown on Ni substrates, using Ni foils as electrodes and described in the text.

an alumina membrane placed on top.²⁹ Deposition was achieved using a pulsed cathodic current technique, with a two-step profile. (The pulsed electrodeposition technique is preferred over the constant current technique because it promotes grain nucleation and avoids diffusion limitations.) The Anodic Aluminium Oxide (AAO) template was then removed. Fig. 12a shows the SEM image of a cross sectional view of uniform, defect-free and self-standing Cu-nanorod current collectors grown directly on to Cu substrate. The length of the nanorods could be varied with deposition time. The width and spacing of the rods are about 200 nm -suitably small to allow over coating with an active material of nanometre thickness while still allowing infiltration of an electrolyte to give an effective diffusion coefficient according to eqn (4). The spacing is too narrow, however, to also allow infiltration of a second electrode and current collector as in the full 3D structure. Therefore the coated nanoarray itself should be considered as a nanocomposite electrode in the semi-3D cell.

Further work developed Ni nanorod arrays (Fig. 12b) as possible current collectors for either anodes or cathodes.³⁰ These were grown directly on Ni substrates using the pulsed cathodic current technique, and a typical Watts bath electrolyte. With longer deposition times, the nanorod arrays tend to form bundles as seen in Fig. 12b. This phenomenon is important for the function of the nanoarray in the 3D device because it represents a hierarchical structure in which electrolyte penetration within the bundles would enhance the effective diffusion coefficient of the composite electrode while the inter-bundle spacing could allow infiltration of a second electrode to give the full 3D configuration.

Aluminium is widely used as the current collector in positive electrode materials, however, this material is not suitable for use as the negative electrode current collector.²⁸ The same approach as for Cu was used to grow Al nanorod current collectors using and Ni nanorods.³¹ The nanorods were deposited using pulsed conditions from ionic liquids onto planar aluminium substrates

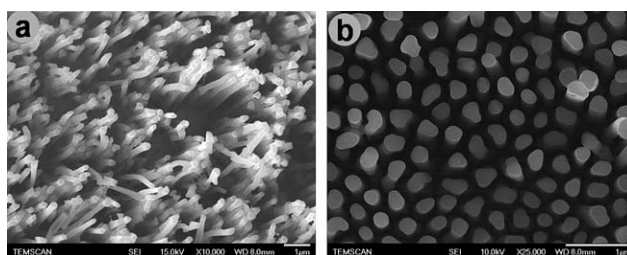
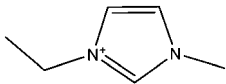
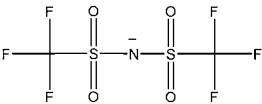
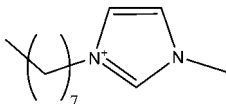
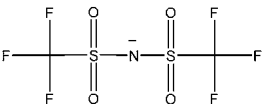
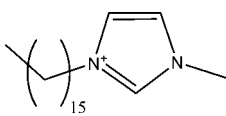
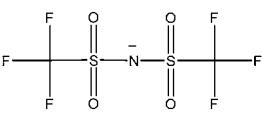


Fig. 13 (a) Oblique-view and (b) top-view SEM images of Al nanorods obtained using optimized pulse-potential conditions.

Table 2 The different ionic liquids used

Ionic liquid	Cation	Anion
[EMIm]TFSI		
[C ₈ MIm]TFSI		
[C ₁₆ MIm]TFSI		

using porous alumina as templates Free standing arrays of aluminium nanorods were obtained after dissolution of the alumina template. SEM images of the substrates formed using this method are shown in Fig. 13.

A novel template-free approach has been used to form a different type of microstructured aluminium current collector.³² Electro-deposits of aluminium were grown on aluminium substrates from AlCl₃-based ionic-liquid electrolytic baths (Table 2).

Using pulse current deposition, the Al deposits had a mole-hill type of morphology which was found to adhere well to the substrate. It was found that the particle size and distance between particles could be controlled to some extent by varying the deposition conditions (ionic liquid-based bath, current density, deposition time, temperature) to form a microstructured electrode ranging in term of particle diameter/interparticle distance from about 0.8 μm/2 μm to 2 μm/7.5 μm respectively (Fig. 14).

A planar Al substrate was oxidised by repetitive cyclic voltammetry, leading to a needle-like morphology (0.8 μm mean height, 0.5 μm diameter and 0.8 μm separation) after 1000 cycles (Fig. 15).³³ The morphological characteristics could be controlled by varying the number of cycles and the potential limits. This template-free process could be considered as a means of

producing nanostructured layer to be placed on a larger, microstructured, current collector of a full 3D battery.

A second etching approach to form Al current collectors has been presented by Nishio *et al.* They use an insulating mask which partially covers the aluminium substrate. An anodic etching in hydrochloric acid is then undertaken to reveal a high aspect ratio honeycomb or pillar like structure depending on which mask is used.^{34,35}

A method for the electroless deposition of Au³⁶ and Ni³⁷ current collectors on microstructured silicon substrates (MCPs discussed earlier) has been developed by Golodnitsky *et al.* For the electroless deposition of Ni a sulfamate-based electrolyte with double complexing/buffering agents produced the highest quality nickel films shown in Fig. 16.

A tetrachloroaurate-thiosulfate electrolyte with sodium ascorbate as reducing agent was used for the electroless deposition of a gold current-collector. Control of the temperature, pH and relative concentration of the electrolyte components gave conformal 3D films on the perforated silicon.

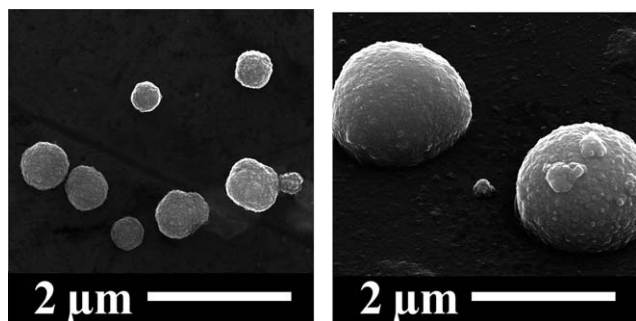


Fig. 14 Different views of the Al ball deposit obtained in a [C₈MIm] TFSI/AlCl₃ medium (molar ratio 1 : 1.6) at RT (left) and a [C₁₆MIm] TFSI/AlCl₃ medium (molar ratio 1 : 2) at 70 °C (right) using pulse current deposition (−4.53 mA cm^{−2} current density, 200 ms pulse, 5s relax, 10min time deposit). Reprinted with permission from ref. 32.

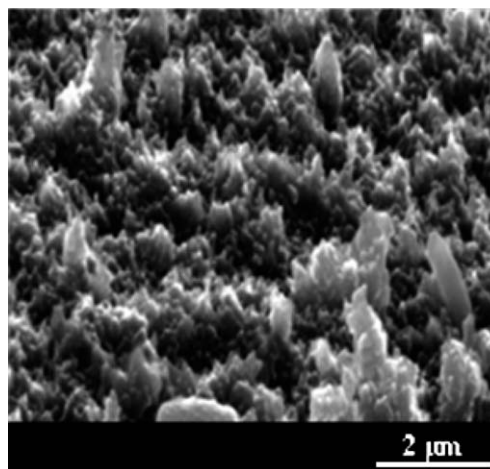


Fig. 15 SEM pictures (tilt of 60°) of a needle-like Al substrate corroded after 1000 cycles in a [EMIm]TFSI/AlCl₃ medium (molar ratio 1/1.5) at RT (cycling between −0.7V and 4V vs. Al^{III}/Al, 100 mV s^{−1} scan rate). Reprinted with permission from ref. 33.

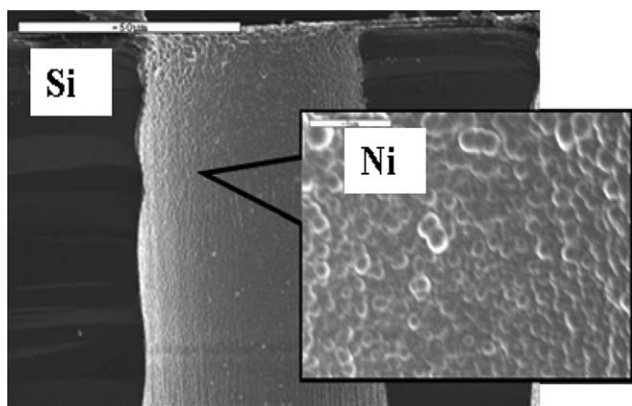


Fig. 16 Electroless Ni current collector on perforated silicon substrate. The 2–4 μm Ni layer is conformal and highly adherent. The scale bars indicate 50 μm on the main image and 5 μm on the inset. Reprinted with permission from ref. 37.

2.2 Positive electrode materials

The following section outlines the various attempts to conformally coat some of the high aspect ratio substrates with the cathode layer.

Conformal deposition of nanostructured LiCoO_2 was obtained on the of Ni and Al nanorods described earlier as current collectors. Nanostructured LiCoO_2 was synthesized by thermal decomposition of sol-gel precursors spray-coated onto the respective nanorod current collectors.³⁸ This process resulted

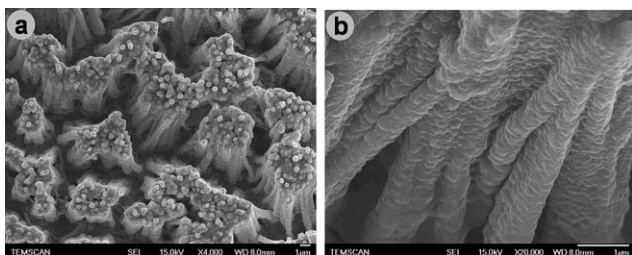


Fig. 17 (a) Low and (b) high magnification SEM images of Ni nanorod-supported LiCoO_2 deposits.

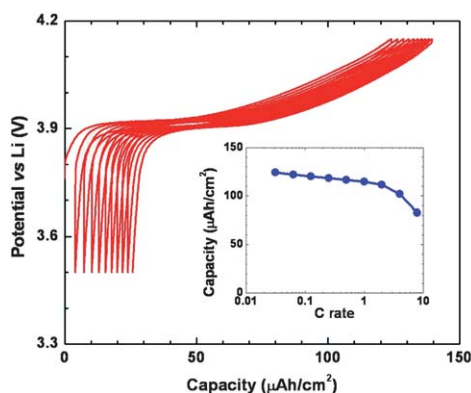


Fig. 18 (a) Charge-discharge galvanostatic curves for aluminium nanorod-supported LiCoO_2 deposits cycled at a rate of $C/10$ versus Li and using a charge cut off voltage of 4.15 V. Inset: rate capability plot for the same electrode. (b) Normalised capacity rate capability plots for Al nanorod-supported LiCoO_2 electrode. LiCoO_2 film deposited on planar Al foil with different thickness (3 and 5 layers of spray-coating).

in the formation of a thick conformal coating of nano-structured LiCoO_2 onto the Ni nanorod arrays shown in Fig. 17.

The same procedure was followed for Al nanorod arrays to obtain Al-nanorod supported LiCoO_2 deposits. Fig. 18a shows a well defined plateau around 3.9 V corresponding to the first-order phase transition between two hexagonal phases (during Li de-insertion and insertion). The cycling shows negligible hysteresis and the electrodes were found to exhibit excellent capacity retention. In Fig. 18b, normalized capacity is plotted versus rate to highlight the high rate performance of 3D positive electrode. Excellent rate capability was observed for the Al nanorod-supported LiCoO_2 electrode compared to their planar counterparts and is shown to recover $\sim 70\%$ of its total capacity at a high rate of 8C.

Thin-film nanosize-particle copper sulfide cathodes³⁶ were electrodeposited on the 3D perforated silicon substrates (Fig. 19) previously used by Nathan *et al.* for the preparation of molybdenum sulfide. The morphology and composition of the cathodes were controlled by varying the operating parameters, such as current density, pH, and temperature, of the electrolyte. The addition of a polymer to the electrolyte bath enabled the formation of sulfur-rich 1–3 micrometre thick porous layers. This was not possible without the additive, which serves to decrease the internal stresses in the bulk of the deposit.

A second cathode has also been developed for use on MCP substrates. V_2O_5 cathodes were prepared by electro-oxidation of a vanadium precursor on 3D-perforated substrates (Fig. 20). As-deposited cathodes had an amorphous structure which crystallised after thermal treatment at 400 °C in air.

Semi-3D cells with Ni or Au current collectors gave capacities between 1.0 to 2.5 mAh cm^{-2} with CuS or V_2O_5 cathodes, depending on the morphology and composition of the cathode; the cells ran for >400 reversible cycles showing low degradation (Fig. 21). The capacity is in good agreement with the geometrical area-gain (A.G.) factor of 9 for the perforated substrate. At constant charge/discharge current, the semi-3DMBs with modified copper sulfide cathode retained approximately 80% of the initial capacity when the discharge rate increases from 120 $\mu\text{A cm}^{-2}$ to 2 mA cm^{-2} . The semi-3D cell with sub-micron thick modified CuS cathode was charged in 0.6 min, *i.e.* at the 100C rate. Under these conditions, however, the capacity of battery is

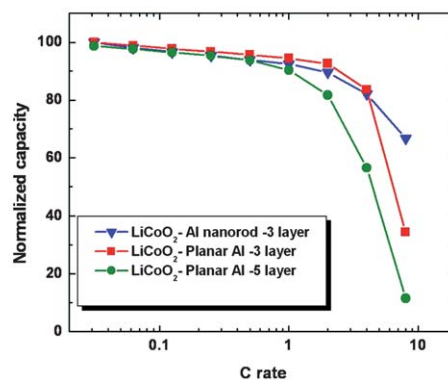




Fig. 19 CuS electrodeposited on perforated (3D) silicon substrates. The scale bars indicate 200 μm on the left most image and 5 μm on the two right most images. The left most image gives a global representation of the deposition over the pores. The two right-most images give an idea of the microscopic differences in the quality of the deposit at the top and in the middle of the channel, indicating a conformal deposition. Reprinted with permission from ref. 36.

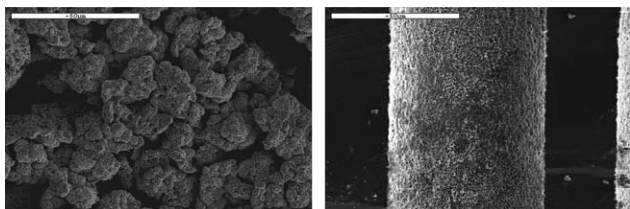


Fig. 20 SEM images of the electrodeposited V_2O_5 cathodes. The scale bars indicate 50 μm .

only 30% of its initial value (Fig. 21). Peak-power capability of 50 mW/cm^2 and a stable electrochemical behavior have been reported for these materials. It is expected that the full 3DCMB may exhibit even better energy density and power capability of 7.4 kW L^{-1} .

Conformal layers of MnO_2 have been deposited onto carbon foam substrates (Fig. 22). As-deposited MnO_2 was found to be inactive to lithium insertion or extraction until a heat treatment was performed at 400 $^\circ\text{C}$ after which a reversible capacity of around 150 mA h g^{-1} was achieved.³⁹ A sub-micron film deposited on a planar current collector showed a reversible capacity per footprint of *ca.* 50 $\mu\text{Ah cm}^{-2}$. Much higher capacities per footprint, up to 10 mA h cm^{-2} , were obtained from 5 μm deposits of MnO_2 on 100 ppi (pores per inch) compressed carbon foams.

2.3 Negative electrode materials

Atomic layer deposition was used to deposit a thin ($\sim 20 \text{ nm}$) and conformal layer of TiO_2 onto the nanorods.³¹ These 3D nanostructured electrodes were cycled vs. Li and showed a footprint capacity which is roughly ten times greater than the same 2D half

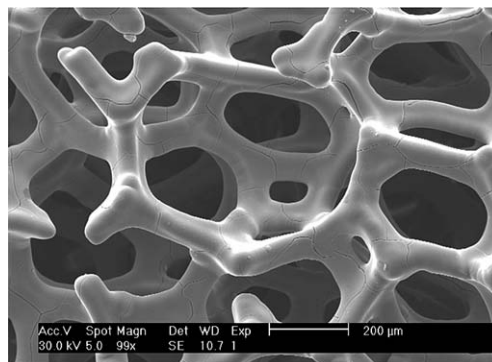


Fig. 22 Conformal MnO_2 film on carbon foam.

cell (TiO_2 deposited on Aluminium plate). They are able to provide approximately 40 and 35% of the initial capacity (cycling at C/5 rate) even when the cycling current has been increased by 50 (10 C) and 100 (20 C) times, respectively. The outstanding performance is the result of the nanostructured active material and the conformal 3D-deposition.

Cu_2Sb was investigated as a negative electrode material on the Cu nanorod substrates discussed earlier.⁴⁰ To prepare nanostructured Cu_2Sb active material the authors electrodeposited Sb and alloyed this with the Cu from nanorod current collector. To promote the diffusion of the electroactive species within the 3D structure and thus to obtain a uniform coverage of the complex 3D surface of the Cu nanorod current collectors, the electrodeposition was performed using pulsed-current steps rather than a simple galvanostatic technique. Homogeneous and conformal Sb deposits (Fig. 23) were obtained under the optimized conditions.

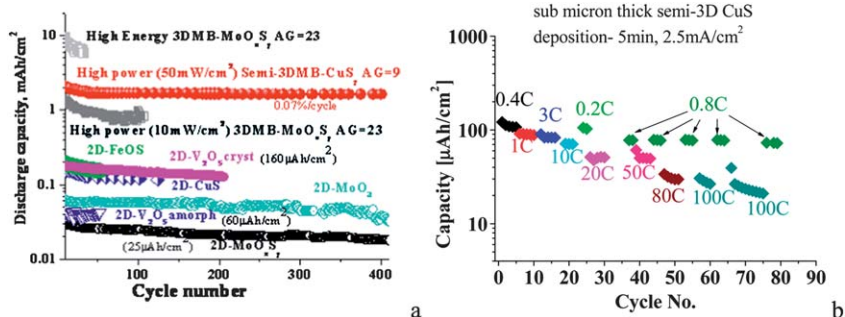


Fig. 21 a) Cyclability of 2D and 3D cells with different cathode materials. b) Capacity vs. discharge current density (C-rate) of a 3D Li/CuS half-cell on a perforated Si substrate.

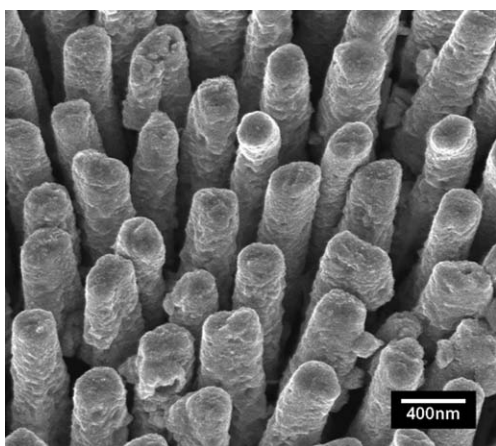


Fig. 23 SEM images of Cu nanorod current collectors coated with Sb under optimized current pulse conditions. Reprinted with permission from ref. 40.

The best performance was observed when an annealing step was used. After the electrodeposition a thermal annealing at 120 °C in vacuum was used to promote full alloying of Sb with the Cu current collectors. As expected, only the Cu₂Sb phase formed regardless of the Cu : Sb atomic ratio. The voltage profile and capacity stability of 3D electrodes annealed for 1h and 12h are shown and compared with non-annealed electrode (Fig. 24). Plateaus typical of Cu₂Sb were observed during lithiation and delithiation. The capacity retention upon cycling is greatly improved (at least doubled) by the annealing step and with the annealing time. The complete formation of the alloy Cu₂Sb which presents lower volume expansion percentage than pure Sb and probably the extended availability of Cu to be re-inserted in the structure are most likely the reasons for the observed increase of the 3D electrode cycling life. The capacities observed were around 300 μA h cm⁻².

2.4 Electrolytes

The following section will look at several different approaches to polymer electrolyte fabrication on the high aspect ratio substrates required for this project. This step is one of the most

difficult when fabricating a 3D microbattery as the coating must be perfect with no cracks or holes that will result in short circuits and problems.

A hybrid co-polymer poly vinylidene fluoride–hexa-fluoropropylene (PVDF-HFP)⁴⁰ has been used for the preparation of polymer electrolyte film onto the nanostructured 3D electrode. Based on the Bellcore process, Dibutyl-phthalate (DBP) plasticizer was added to the polymer to increase its liquid electrolyte uptake (and thus its ionic conductivity) and to create open porosity that will favour a rapid impregnation of the liquid electrolyte. In order to obtain a thin film with homogenous composition they focused on the co-synthesis of an inorganic compound and the polymer. 3-glycidyloxypropyl trimethoxy-silane (GPTMS) was selected as SiO₂ precursor, to increase the polymer mechanical properties and the liquid electrolyte uptake ability. A hydrolysis step followed by poly-condensation to form the inorganic network was used.

Prior to its *in situ* synthesis on 3D electrodes, the hybrid polymer separator was prepared on planar stainless steel electrode in order to evaluate its performance as Li-ion battery electrolyte. The hybrid polymer film was also deposited onto the 3D nanostructured Cu₂Sb electrode by a spray-coating technique and the SEM images revealed a thin polymer layer deposited onto the 3D electrode arrays (Fig. 25).

Solid-state polymer materials are ideal as electrolyte for many of the 3D-microbattery applications currently under study, not least in terms of safety combined with mechanical flexibility. The low conductivity identified as an obstacle for the use of polymer electrolytes for conventional batteries is less of a problem in these devices, since the electrolyte layer is very thin. However, it is not trivial to cast polymers conformally onto complex structures.

Poly(acrylonitrile) (PAN) films of controlled thickness were deposited directly onto glassy carbon, nickel foam and MnO₂ substrates by cathodic electropolymerisation of acrylonitrile in acetonitrile with tetrabutylammonium perchlorate (TBAP) as the supporting electrolyte.⁴⁵ The electronic barrier properties of the films were confirmed by impedance spectroscopy of carbon | PAN | Hg cells while the ionic resistance of the films varied from 200 kΩ cm² in the dry state to 1.4 Ω cm² when plasticised with 1 M LiPF₆ in propylene carbonate. A galvanic cell was prepared by successive electrodepositions of MnO₂ and PAN on a carbon

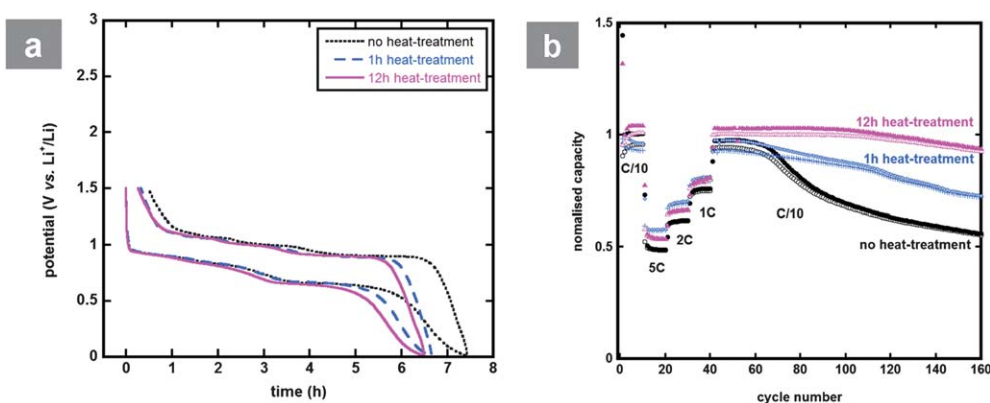


Fig. 24 (a) Cycling profile (5th cycle) and (b) capacity retention upon cycling of 3D Cu₂Sb electrodes annealed at 120 °C for 1h and 12h. The non-annealed electrodes are also compared. Reprinted with permission from ref. 40.

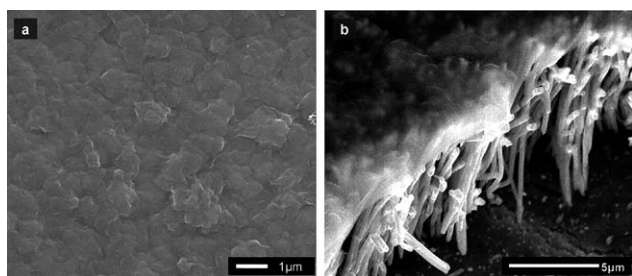


Fig. 25 (a) Top and (b) cross-sectional views of SEM micrographs of a hybrid polymer electrolyte synthesised onto a 3D nano-structured Cu electrode. Reprinted with permission from ref. 40.

substrate, using liquid lithium amalgam as the top contact. The cell showed a stable open circuit potential and behaved normally under the galvanostatic intermittent titration technique (GITT).

Another successful approach used by Tan *et al.*⁴¹ has been building on the use of oligomeric poly(ether amine) (PEA), which previously has been shown to form ultrathin layers ($\sim 10 \text{ \AA}$) onto LiFePO_4 cathode particles, thereby resulting in a capacity enhancement.^{42,43} PEA has surfactant properties, forming hydrogen bonds between the amine groups and oxide atoms at the electrode surfaces, and therefore uniformly follows the substrate. Tan and co-workers blended PEA with a PPO-diacrylate, which could be *in situ* cross-linked by UV-radiation in presence of an initiator, thereby providing enough mechanical stability in the resulting LiTFSI-based electrolyte layer. The resulting electrolyte formed 1–3 μm thick coatings, following the contours of LiFePO_4 particle surfaces (see Fig. 26), and displayed a conductivity of $3.5 \times 10^{-6} \text{ S cm}^{-1}$ at room temperature. Batteries constructed *vs.* Li could be cycled for at least 30 cycles,

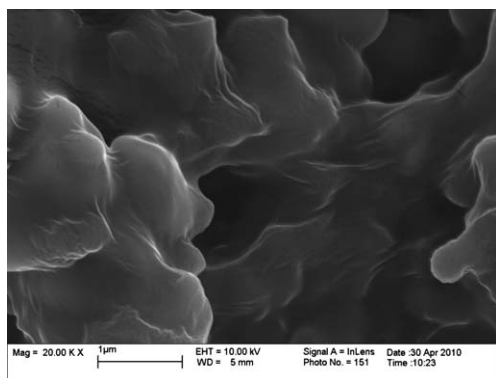


Fig. 26 SEM micrographs of a LiFePO_4 cathode coated with a cross-linked PEA/PPO-diacrylate blend electrolyte (top view). Reprinted with permission from ref. 41.

although only displaying normal capacities at low cycling rates and elevated temperatures ($60 \text{ }^\circ\text{C}$), probably due to high interfacial resistance.⁴¹

A totally different approach to the above has been to fabricate the separator between interlaced pores in a rigid Si substrate, which also acted as micro-containers for the electrode materials (Fig. 27).⁴⁴ The silicon separating the micro-containers was converted into a nanoporous separator (membrane) by a metal-assisted anisotropic wet-etching process. The apparent “effective” ionic conductivity (σ_{eff}) of the liquid electrolyte trapped in the interlaced mesoporous membrane was found to be inversely proportional to the pore size, varying from 0.07 to 0.24 mS cm^{-1} , which is 5–18 times lower than the ionic conductivity of LiPF_6 EC:DEC electrolyte in Li/Celgard/Li cell. This conductivity suppression was assigned to the mesoporous structure of the silicon membrane with complex ion-transport paths, for which the interconnectivity of pores and therefore the tortuosity become relevant parameters.

2.5 Summary of fabrication methods

Fabrication of the microstructured current collectors as substrates for interdigitated or network electrodes has been achieved by several methods. The lithography methods have the advantage that in principle, they can be applied to production to a wide range of dimensional specifications. In particular, the column or pore thickness can be large enough for subsequent deposition of electrode and polymer electrolyte while leaving ample space for backfilling with the second electrode. The use of carbon foam has also been shown to be a cheap alternative microstructured current collector with a rather large pore size of $100 \mu\text{m}$. Both types of electrodes offer large aspect ratios, and carbon (or a metal) foam offers almost unlimited overall dimensions.

Various electrodeposition methods have achieved a range of current collector arrays with small pore sizes and the template methods offer a good control of the geometries. The template-free methods are conceptually attractive, although further development will be required in order to improve the morphology and pore size for use as current collectors suitable for the subsequent conformal deposition of the other components required in the interdigitated configuration. These materials are, however, well suited as supports for nanostructured electrodes, either in semi-3D cells or as coatings over micro-column arrays in a 3D cells with hierarchically structured, interpenetrating electrodes. All of the materials described showed good compatibility with the applications as either negative, or positive current collectors.

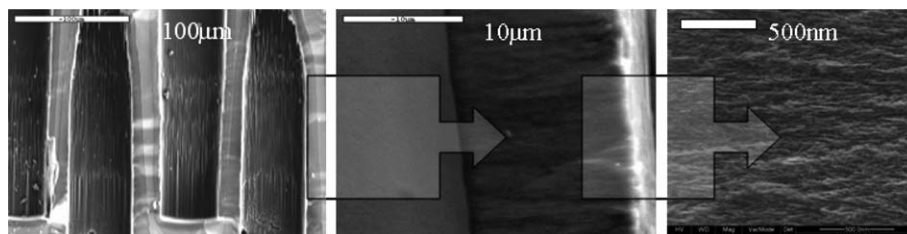


Fig. 27 SEM and ESEM images of interlaced silicon sample with porous partition.

The electrodeposition of the first layer of electrode material has been most successful, with demonstrations of conformal coatings of several active materials that will provide sufficient capacity to meet the specifications and electrochemical characterization in half cells has generally met target specifications.

Electrodeposition of polymers has been demonstrated, and conformal, largely pinhole-free layers around the target thickness of one to a few microns have been achieved. Other deposition methods such as infiltration and UV curing have produced successful coatings, although pinhole-free layers have not yet been demonstrated. The area of producing conformal and pinhole free layers remains an important challenge in the layered deposition approach. The alternative of starting with a microfabricated porous ceramic is attractive for small devices.

The most important outstanding task is backfilling with the second electrode and making good electronic contact. As mentioned above, this has been achieved for MCMB (carbon) by successive steps of impregnation from a slurry followed by drying (22), thus completing a 3D battery structure which showed 1 mAh cm⁻². Since then little progress has been reported for this critical final step although the same concept could be applied to any electrode in powdered form, provided it has an electronically conducting surface. Therefore we can look forward to many innovative solutions to this problem in the near future.

3. Conclusions

Many possible configurations and designs for 3D batteries, semi-3D batteries and 2D batteries have been investigated and the principles of design for high discharge rate have been described. Research into these configurations has produced several methods of providing, as a starting point for cell fabrication, arrays of nanopillar current collectors on a substrate. Copper current collectors can be produced for anode support, aluminium for cathodes and nickel, which may be suitable for either given a suitable electrolyte to avoid corrosion. Conformal deposition of active materials has been successful in the case of cathodes and anodes of TiO₂, SnO₂ and Cu₂Sb have also been deposited conformally. Methods for conformal deposition of electrolytes have comprised solvent-assisted impregnation, electropolymerisation, and electrophoresis. The final step of filling the remaining volume with a second electrode has been achieved by infiltration, but no technique has yet emerged for enhancing the conductivity of the second electrode with a continuous metallic conductor. The alternative strategies of starting with a monolithic substrate with unidirectional, interlaced and random 3D (sponge) pores have progressed by application of conformal coating methods.

Acknowledgements

The authors would like to thank the EU FP7 Theme 4: NMP project SUPERLION (www.superlion.eu) for continued support. The authors would also like to extend their personal thanks to Professor Josh Thomas for his enthusiastic encouragement.

References

- 1 J. W. Long, B. Dunn, D. R. Rolison and H. S. White, *Chem. Rev.*, 2004, **104**, 4463–92.
- 2 D. R. Rolison, J. W. Long, J. C. Lytle, A. E. Fischer, C. P. Rhodes, T. M. McEvoy, M. E. Bourg and A. M. Lubers, *Chem. Soc. Rev.*, 2009, **38**, 226–52.
- 3 J. Bates, N. J. Dudney, B. Neudecker, A. Ueda and C. D. Evans, *Solid State Ionics*, 2000, **135**, 33–45.
- 4 J. Souquet and M. Duclot, *Solid State Ionics*, 2002, **148**, 375–379.
- 5 R. W. Hart, H. S. White, B. Dunn and D. R. Rolison, *Electrochem. Commun.*, 2003, **5**, 120–123.
- 6 S. Jones and J. Akridge, *J. Power Sources*, 1995, **54**, 63–67.
- 7 K. Xu, *Chem. Rev.*, 2004, **104**, 4303–417.
- 8 H. Kim, R. Auyeung and A. Pique, *J. Power Sources*, 2007, **165**, 413–419.
- 9 J. R. Owen, *Chem. Soc. Rev.*, 1997, **26**, 259–267.
- 10 P. Johns, M. Roberts, Y. Wakizaka, J. H. Sanders and J. Owen, *Electrochem. Commun.*, 2009, **11**, 2089–2092.
- 11 M. D. Fleischauer, J. Li and M. J. Brett, *J. Electrochem. Soc.*, 2009, **156**, A33.
- 12 G. Teixidor, R. Zaouk, B. Park and M. Madou, *J. Power Sources*, 2008, **183**, 730–740.
- 13 D. Tonti, M. J. Torralvo, E. Enciso, I. Sobrados and J. Sanz, *Chem. Mater.*, 2008, **20**, 4783–4790.
- 14 B. G. Park, S. Kim, I.-D. Kim and Y. J. Park, *J. Mater. Sci.*, 2010, **45**, 3947–3953.
- 15 F. Jiao and P. G. Bruce, *Adv. Mater.*, 2007, **19**, 657–660.
- 16 A. H. Whitehead, J. M. Elliott, J. R. Owen and G. S. Attard, *Chem. Commun.*, 1999, 331–332.
- 17 K. Dokko, J. Sugaya, H. Nakano, T. Yasukawa, T. Matsue and K. Kanamura, *Electrochem. Commun.*, 2007, **9**, 857–862.
- 18 V. Zadin, D. Brandell, H. Kasemägi, A. Aabloo and J. O. Thomas, *Solid State Ionics*, 2010, DOI: 10.1016/j.ssi.2010.02.007.
- 19 V. Zadin, H. Kasemägi, A. Aabloo and D. Brandell, *J. Power Sources*, 2010, **195**, 6218–6224.
- 20 L. Baggetto, J. F. M. Oudenhoven, T. van Dongen, J. H. Klootwijk, M. Mulder, R. A. H. Niessen, M. H. J. M. de Croon and P. H. L. Notten, *J. Power Sources*, 2009, **189**, 402–410.
- 21 P. H. L. Notten, F. Roozeboom, R. A. H. Niessen and L. Baggetto, *Adv. Mater.*, 2007, **19**, 4564–4567.
- 22 J. F. M. Oudenhoven, L. Baggetto and P. H. L. Notten, *Adv. Energy Mater.*, 2011, **1**, 10–33.
- 23 H.-S. Min, B. Y. Park, L. Taherabadi, C. Wang, Y. Yeh, R. Zaouk, M. J. Madou and B. Dunn, *J. Power Sources*, 2008, **178**, 795–800.
- 24 C. Wang, L. Taherabadi, G. Jia, M. Madou, Y. Yeh and B. Dunn, *Electrochem. Solid-State Lett.*, 2004, **7**, A435.
- 25 K. Kinoshita, X. Song, J. Kim and M. Inaba, *J. Power Sources*, 1999, **81**–**82**, 170–175.
- 26 M. Nathan, D. Golodnitsky, V. Yufit, E. Strauss, T. Ripenbein, I. Shechtman, S. Menkin and E. Peled, *J. Microelectromech. Syst.*, 2005, **14**, 879–885.
- 27 M. Kotobuki, Y. Suzuki, H. Munakata, K. Kanamura, Y. Sato, K. Yamamoto and T. Yoshida, *J. Electrochem. Soc.*, 2010, **157**, A493.
- 28 A. H. Whitehead and M. Schreiber, *J. Electrochem. Soc.*, 2005, **152**, A2105.
- 29 P. Taberna, S. Mitra, P. Poizot, P. Simon and J.-M. Tarascon, *Nat. Mater.*, 2006, **5**, 567–73.
- 30 Y. Lei, B. Daffos, P. Taberna, P. Simon and F. Favier, *Electrochim. Acta*, 2010, **55**, 7454–7459.
- 31 S. K. Cheah, E. Perre, M. Rooth, M. Fondell, A. Härsta, L. Nyholm, M. Boman, J. Lu, P. Simon and K. Edstrom, *Nano Lett.*, 2009, **9**, 3230–3233.
- 32 C. Lecoer, J.-M. Tarascon and C. Guery, *J. Electrochem. Soc.*, 2010, **157**, A641.
- 33 C. Lecoer, J. M. Tarascon and C. Guery, *Electrochem. Solid-State Lett.*, 2011, **14**, A6–A9.
- 34 K. Nishio, T. Fukushima and H. Masuda, *Electrochem. Solid-State Lett.*, 2006, **9**, B39.
- 35 K. Nishio, T. Fukushima, A. Takeda and H. Masuda, *Electrochem. Solid-State Lett.*, 2007, **10**, C60.
- 36 H. Mazon, D. Golodnitsky, L. Burstein and E. Peled, *Electrochem. Solid-State Lett.*, 2009, **12**, 232–235.
- 37 T. Ripenbein, D. Golodnitsky, M. Nathan and E. Peled, *J. Appl. Electrochem.*, 2009, **40**, 435–444.

-
- 38 M. M. Shaijumon, E. Perre, B. Daffos, P. Taberna, J.-M. Tarascon and P. Simon, *Adv. Mater.*, 2010, **22**, 4978–4981.
- 39 P. Johns, M. R. Roberts and J. R. Owen, *J. Mater. Chem.*, 2011, submitted.
- 40 E. Perre, P. L. Taberna, D. Mazouzi, P. Poizot, T. Gustafsson, K. Edström and P. Simon, *J. Mater. Res.*, 2010, **25**, 1485–1491.
- 41 S. Tan, S. Walus, J. Hilborn, T. Gustafsson and D. Brandell, *Electrochem. Commun.*, 2010, **12**, 1498–1500.
- 42 C. Sisbandini, D. Brandell, T. Gustafsson and L. Nyholm, *J. Electrochem. Soc.*, 2009, **156**, A720.
- 43 C. Sisbandini, D. Brandell, T. Gustafsson and J. Thomas, *Electrochem. Solid-State Lett.*, 2009, **12**, A99–101.
- 44 T. Ripenbein, D. Golodnitsky, M. Nathan and E. Peled, *Electrochim. Acta*, 2009, **56**, 37–41.
- 45 G. El-Enany, M. J. Lacey, P. A. Johns and J. R. Owens, *Electrochem. Commun.*, 2009, **11**, 2320.
-